

OPEN ENDED EXPERIMENT

TENSILE TESTING OF ACRYLIC WITH GEOMETRIC DISCONTINUITY

ENGR 302 – Experimental Analysis

San Francisco State University

20th December 2024

Abstract

This study examined the tensile behavior of 1/4-inch acrylic specimens with geometric discontinuities. Testing revealed that discontinuities significantly reduced tensile strength and ductility, with control specimens yielding at 11.1 MPa, approximately 80% lower than the manufacturer's specified value. Circular and notched specimens showed better performance, yielding at 18.96 MPa and 21.56 MPa, respectively, with stress concentration factors of 1.71 and 1.94. In contrast, square and diamond specimens exhibited greater vulnerability, yielding at 17.25 MPa and 20.51 MPa, respectively, with sharp corners amplifying stress concentrations. The findings highlight the critical influence of geometry on material performance and suggest further research to refine predictive models and enhance structural design.

Tom Boivin, Leonard Chau, Driss Hakkou, & Denise Steffen

Table of Contents

Introduction.....	2
Apparatus and Test Procedure.....	3
Results and Discussion	6
Conclusion and Recommendations.....	12
References.....	15
Appendices.....	16
Appendix A	16
Appendix B	16
Appendix C	17
Appendix D	22

Introduction

The tensile strength of a material is a fundamental property that describes its ability to resist breaking under tensile forces. For real-world components, geometric discontinuities such as holes, notches, and other abrupt changes in cross-sectional area often create localized stress concentrations, which amplify the stress beyond what is predicted by simple tensile stress equations [1], [2]. These localized stress amplifications are quantified using the stress concentration factor K_t , which relates the maximum stress at the discontinuity to the nominal stress in the component. Accurate calculation of tensile strength, especially for materials with discontinuities, is essential for predicting failure and ensuring safe structural design.

This experiment measures the tensile strength of 1/4-inch acrylic specimens with various discontinuities and compares the experimental results with theoretical predictions calculated using established methods. For simple geometries, such as circular holes, the stress concentration factor and yield stress can be determined from established charts and equations derived from experimental data. For more complex geometries, such as square hole and diamond-shaped discontinuities, the calculation of stress concentration factors requires a more detailed analysis, including experimental or numerical techniques [2]. Additionally, stress intensity factors (SIFs) derived from fracture mechanics may be applied to evaluate stress at crack tips and assess failure behavior, but are out of the scope of our expertise and thus this experiment.

Acrylic, commonly considered a brittle material, is ideal for this investigation due to its tendency to fail without significant plastic deformation, allowing elastic theory to remain valid until failure. However, it's important to note that acrylic exists in various grades and formulations, such as cast and extruded types, each exhibiting different mechanical properties. For instance, cast acrylic typically offers higher optical clarity and better machinability, while extruded acrylic is more cost-effective but may

have reduced strength and optical properties. In this experiment, we utilized a 1/4-inch-thick cast acrylic sheet, specifically McMaster-Carr part number 4615T47. This material is known for its excellent optical clarity, good tensile strength, and resistance to scratches and scuffs across a wide temperature range [3]. These characteristics make it suitable for applications requiring both aesthetic quality and structural integrity. Understanding the specific properties of the acrylic used is crucial for accurately interpreting the experimental results and their applicability to real-world scenarios. By combining theoretical calculations and experimental data from the Instron Tensile Test system, this study will determine the tensile strength of the material while evaluating the effects of discontinuity geometry on stress distribution and failure. The results will contribute to a deeper understanding of the relationship between stress concentration factors and material strength, providing valuable insights for the design and analysis of components subjected to tensile loading.

Apparatus and Test Procedure

The tensile strength of the acrylic specimens was determined using an Instron Tensile Test System (Model 3369), equipped with a 50 kN load cell for precise force measurement. The apparatus included threaded side-action grips designed to securely hold the 1/4-inch acrylic specimens during testing, ensuring proper alignment and preventing slippage. The Bluehill Universal software facilitated real-time data acquisition and analysis, providing detailed load and elongation measurements throughout the testing process.

The specimens were carefully prepared to ensure accurate evaluation of the effects of discontinuities. Acrylic “dog bone” specimens (Figure 1), including control specimens and those with circular hole, notched, square hole, and diamond hole discontinuities, were 3D modeled and traced using a laser cutter to study stress concentration effects. The gauge area was approximately 67.51 mm^2 (0.105

in^2) for the control specimens and 29.48 mm^2 (0.0457 in^2) for those with discontinuities, while the gauge length (l_0) was approximately 73.38 mm (2.89 inches) for all specimens. However, the inclusion of discontinuities resulted in localized reductions in cross-sectional area, which were accounted for during stress calculations. The surfaces of the specimens were sanded to remove any machining marks or irregularities that could influence stress distribution. Each specimen's dimensions were recorded to calculate the cross-sectional area to account for any discrepancies between test runs. Two trials for each category of discontinuity or control were tested. The detailed dimensions and cross-sectional area for each specimen are provided in Appendix A and Appendix B and a detailed schematic for each discontinuity and control specimen is shown in Figure 2.

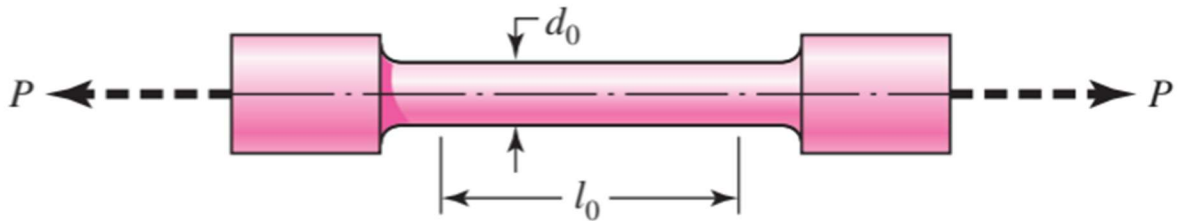


Figure 1: A typical tension-test specimen (also known as a "dog bone" specimen) where d_0 is the original diameter, l_0 is the gauge length, and P is the load applied to the specimen. [2]

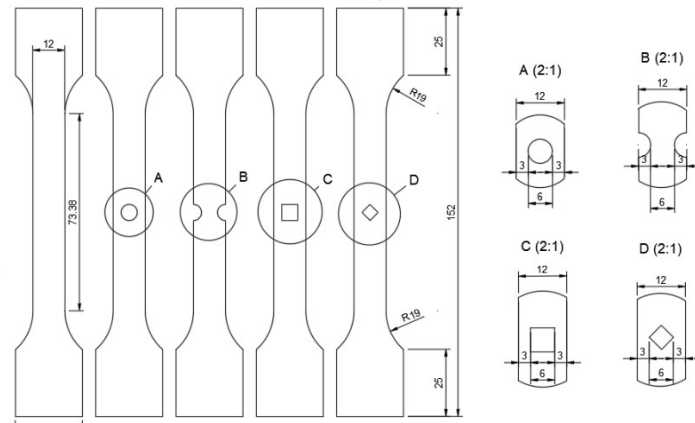


Figure 2: Nominal dimensions of control, circular hole, notched, square hole, and diamond hole specimens

Before testing began, the Instron system was calibrated to ensure accuracy. The grips were adjusted to accommodate the specimen dimensions, applying even clamping pressure to avoid introducing pre-test stresses. Each specimen was mounted between the grips and aligned with the vertical axis of the testing machine to prevent bending or torsional effects. During testing, each specimen was pulled apart at a constant crosshead speed of 2 in/min. The Instron system continuously recorded the tensile load and displacement data until the specimen fractured.

During the experiment, experimental tensile stresses were calculated using the loads recorded and the critical cross-sectional area of the discontinuity or control specimen. The experimental tensile strength σ_t was determined using the equation $\sigma_t = \frac{F}{A}$, where F is the maximum force applied, and A is the critical cross-sectional area of the specimen. Other experimental parameters that were collected are modulus of elasticity, elongation, ultimate stress, and fracture stress. Plots were generated by the Bluehill Universal Software for the Instron Machine of the force applied versus distance elongated for each specimen are in Appendix C. The stress concentration factors (SCFs) relative to the control specimens were calculated for the specimens with circular holes and notches using the equation $K_t = \frac{\sigma_{max}}{\sigma_{nom}}$, where σ_{nom} is the yield stress experienced in a control specimen, and σ_{max} is the yield stress experienced in a specimen with a discontinuity.

Following each test, the fracture surfaces were inspected to identify failure modes, such as brittle fracture or stress concentration effects, and comparisons were made to assess the influence of discontinuity shapes on the material's tensile strength and failure mode. For this experiment, each discontinuity type (control, circular hole, notched, square hole, and diamond hole) was tested twice to ensure the consistency of the results. Observations from these tests were analyzed to identify trends and assess the impact of each discontinuity type on failure behavior.

Results and Discussion

The yield stress of the control specimens was determined to be an average of 11.1 MPa (1611 psi), which is significantly lower than the manufacturer-specified yield stress of 55 MPa (8000 psi) for acrylic [3]. This discrepancy, amounting to an approximate 80% reduction, is detailed in Table 1, where the experimental and theoretical values are compared. Possible reasons for this discrepancy include material degradation, imperfections introduced during manufacturing or the laser cutting process, and environmental factors such as temperature and humidity during testing. These factors likely influenced the material's performance, highlighting the sensitivity of acrylic to external variables. Despite these factors, the control specimens provided a reliable baseline for evaluating the effects of geometric discontinuities.

Table 1: Averaged Yield Stress from Control specimen compared to manufacturers tested yield stress

Manufacturer and Control Comparison	Control
Average Theoretical Yield Stress (MPa)	55.16
Average Actual Yield Stress (MPa)	11.11
% Diff of Yield Stress	79.77

For specimens with geometric discontinuities, the theoretical and experimental results were analyzed to assess tensile behavior, as summarized in Tables 2 and 4 and illustrated in Figures 3 and 4. The theoretical values are averaged due to the slight differences in discontinuity measurements between trial specimens. Circular hole specimens had an experimental yield stress of 18.96 MPa and a stress concentration factor, K_t , of 1.71, closely aligning with theoretical predictions. Notched specimens performed slightly better, with an experimental yield stress of 21.56 MPa and $K_t = 1.94$. Hand calculations for these results are located in Appendix D. These results suggest that notches, despite their

geometric complexity, distribute stress more evenly than circular holes, resulting in marginally higher resistance to tensile loads. In contrast, sharp discontinuities such as square and diamond geometries significantly weakened the material. The diamond-shaped specimens demonstrated the poorest performance, with a yield stress of 17.24 MPa and ultimate stress of only 34.70 MPa, while square specimens failed at the corners due to crack propagation.

Table 2: Average theoretical values for Control, Square Hole, and Notched specimens

Theoretical Data	Control	Square Hole	Notched
Average Theoretical Yield Force (N)	750.01	726.12	572.37
Average Theoretical Yield Stress with Control Yield Stress as Nominal (MPa)	11.11	23.70	19.74
Average Theoretical Concentration Factor (K_t)	1.00	2.13	1.78

Table 3: Averaged experimental data

Experimental Data	Control	Circle Hole	Notched	Square	Diamond
Average Actual Yield Force (N)	750.00	580.00	625.00	500.00	600.00
Average Actual Cross-Sectional Area (mm²)	67.51	30.64	29.00	29.00	29.30
Average Actual Yield Stress (MPa)	11.11	18.96	21.56	17.25	20.51
Average Actual Ultimate Stress (MPa)	57.04	50.27	71.63	54.77	34.70
Average Actual Fracture Stress (MPa)	51.84	50.27	71.57	54.77	34.70
Average Actual Elongation at Yield (mm)	0.55	0.45	0.48	0.39	0.44
Average Actual Maximum Elongation (mm)	10.20	1.63	2.25	1.76	0.89
Average Modulus of Elasticity (MPa)	1743.00	4116.50	4098.50	3483.00	4478.00
Average Actual Concentration Factor (K_t)	1.00	1.71	1.94	no data	no data

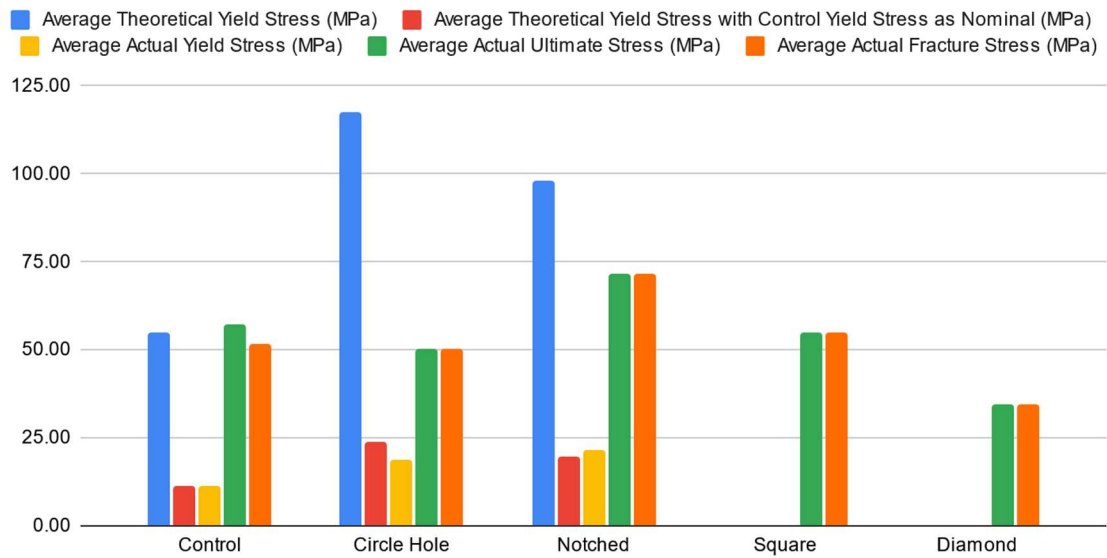


Figure 3: The average theoretical and experimental values of yield stress, fracture stress, and ultimate stress for all specimens

A key distinction between specimens with discontinuities and the control specimens lies in the relationship between fracture stress and ultimate stress. In specimens with discontinuities, the fracture stress was approximately equal to the ultimate stress, indicating a brittle failure with minimal energy absorption after yielding. By contrast, the control specimens experienced a reduction in stress after ultimate stress was reached, reflecting elastic deformation before complete failure. This behavior suggests that discontinuities significantly reduce the ability of specimens to deform before fracture.

Figure 3 illustrates these trends, showing the elongation of each specimen at the point of yielding and at fracture. Control specimens exhibited a maximum elongation of 10.2 mm, while circular hole specimens elongated only 1.63 mm, and diamond specimens elongated a mere 0.89 mm. These results underscore the brittleness induced by stress concentrations, making specimens with discontinuities far more prone to sudden failure.

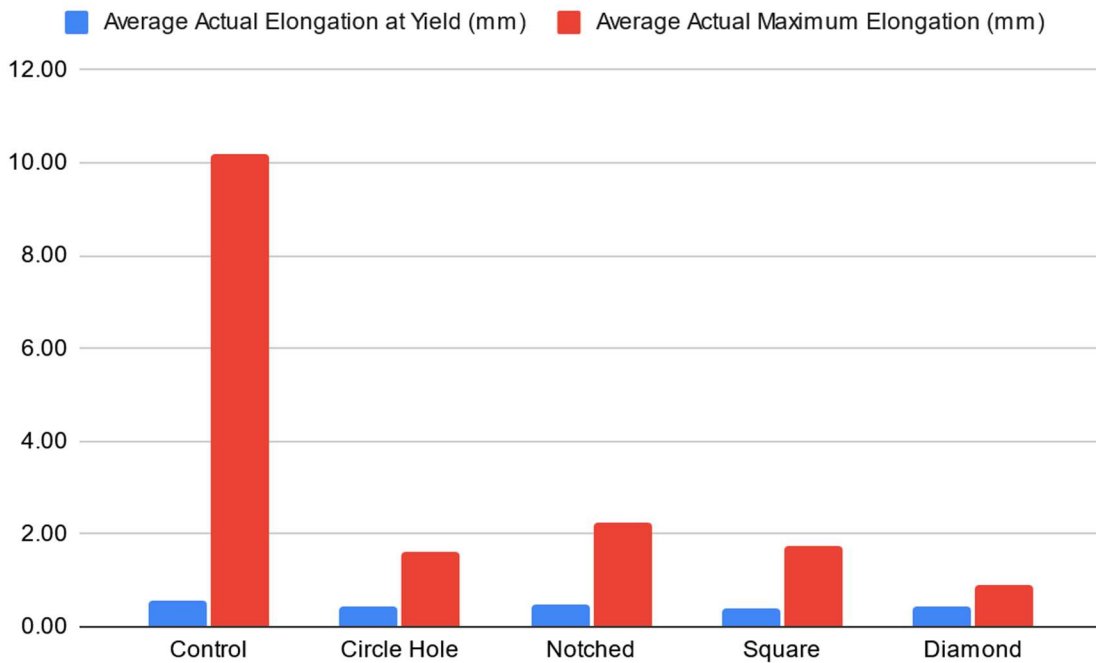


Figure 4: Elongation of each specimen at yielding and at fracture

The modulus of elasticity, presented in Table 4, reinforces these findings. Diamond-shaped specimens exhibited the highest modulus at 4478 MPa, reflecting increased stiffness but reduced strain capability, while the control specimens had a modulus of 1743 MPa, indicating their comparatively higher ability to absorb deformation. Visual inspection of fracture surfaces further supported these results. Control specimens displayed a visible color change from translucent to opaque white near the fracture site, a sign of significant elastic deformation before failure. In contrast, specimens with discontinuities failed with minimal warning or deformation, with fractures initiating at stress concentration points, as shown in Figure 4. Sharp corners in square and diamond specimens acted as stress amplifiers, leading to predictable failure patterns and underscoring the role of geometry in amplifying stress (Figure 5).



Figure 5: Photo of failed specimens. From left to right: diamond hole, square hole, notch, circle hole, control.

Finally, the comparison of theoretical and experimental stress concentration factors showed strong agreement for simpler geometries like circular holes, with deviations of less than 20%, as shown in Table 4. However, for complex shapes like squares and diamonds, the absence of established theoretical models led to greater deviations, highlighting the need for further study. These findings, summarized in Tables 3 and 4, emphasize the critical influence of geometry on material strength and point to the necessity of improved predictive tools for unconventional discontinuities.

Table 4: Comparison of actual and theoretical values of stress concentration factor

Actual and Theoretical Comparison	Control	Circle Hole	Notched
Ratio of Actual vs Theoretical (Yield Force \propto Yield Stress \propto Stress Concentration Factor)	100.00%	125.08%	91.55%
Percent Error	0.00%	-20.02%	9.25%

Conclusion and Recommendations

This experiment successfully analyzed the tensile behavior of 1/4-inch acrylic specimens with geometric discontinuities. The study confirmed the significant impact of discontinuities on material strength, ductility, and failure mechanisms. Control specimens provided a baseline yield stress of 11.1 MPa, which was 80% lower than the manufacturer-specified value of 55 MPa, highlighting potential influences from material degradation, laser cutting imperfections, or environmental testing conditions.

Specimens with circular holes and notches exhibited increased stress concentration factors of 1.71 and 1.94, respectively, compared to the control specimens, as predicted theoretically. These geometries demonstrated higher resistance to failure than square and diamond-shaped discontinuities, which featured sharp corners acting as pre-existing cracks. Diamond specimens performed the worst, with a yield stress of 17.25 MPa and ultimate stress of only 34.70 MPa, reflecting their heightened vulnerability to stress concentrations. Additionally, elongation data revealed that specimens with discontinuities lost significant ductility, with maximum elongation dropping from 10.2 mm in control specimens to just 0.89 mm in diamond-shaped specimens.

The relationship between fracture stress and ultimate stress further differentiated the behavior of control specimens and those with discontinuities. Control specimens showed a reduction in stress after reaching ultimate stress, indicative of elastic deformation, while discontinuity specimens fractured at stress levels nearly identical to their ultimate stress, underscoring their brittle failure modes. These findings, supported by visual analysis of fracture surfaces, illustrate how discontinuities amplify stress concentrations and compromise material performance.

Despite strong alignment between theoretical and experimental results for simple geometries, such as circular holes and notches, deviations were noted for complex geometries like squares and diamonds. These findings emphasize the need for improved theoretical models to accurately predict stress distribution and failure mechanisms in unconventional discontinuities.

To enhance the accuracy and applicability of future experiments, several recommendations are proposed. First, reducing the crosshead speed from 2 in/min to 0.5 in/min is advised, as a slower rate could minimize dynamic effects and allow for more precise stress-strain measurements, particularly for brittle materials like acrylic. Additionally, conducting tensile tests under varying temperatures would provide valuable insights into acrylic's behavior in different environmental conditions. For example, the material's brittleness is likely to increase in colder conditions, further emphasizing the effects of stress concentrations.

Improving preparation techniques could also enhance the consistency and reliability of results. Refining the laser cutting process and surface finishing would reduce imperfections that amplify stress concentrations, while polishing the sharp edges of discontinuities could mitigate crack initiation and propagation. In addition, extending the theoretical analysis by developing or referencing stress intensity factor (SIF) models for complex geometries, such as squares and diamonds, would deepen the

understanding of failure mechanisms. Complementing experimental results with numerical simulations, such as finite element analysis (FEA) [2], would strengthen the study's theoretical foundation.

Exploring alternative materials with varying mechanical properties, such as ductile plastics or composites, could shed light on how geometric discontinuities affect different material behaviors. Comparisons between brittle and ductile materials would be particularly useful for informing design decisions in engineering applications. Broadening the scope of discontinuities to include shapes like ellipses, star patterns, or irregular geometries would provide a more comprehensive understanding of how different geometries influence tensile performance. These recommendations collectively aim to refine the experimental process and expand its applicability to a wider range of materials and scenarios.

This study emphasizes the importance of considering geometric discontinuities in the design and analysis of structural components. By integrating the insights gained into material selection and geometry optimization, engineers can mitigate premature failure and enhance the safety and durability of structural systems.

References

- [1] T. L. Anderson, *Fracture Mechanics: Fundamentals and Applications, Third Edition*. CRC Press, 2005.
- [2] R. Budynas and K. Nisbett, *Shigley's Mechanical Engineering design*. McGraw-Hill Science/Engineering/Math, 2010.
- [3] "McMaster-Carr." <https://www.mcmaster.com/4615T47/>
- [4] "Stress Concentration Calculator | MechaniCalc." <https://mechanicalc.com/calculators/stress-concentration/>

Appendices

Appendix A

Measured Dimensions and Calculated Cross-Sectional area for Control, Circle Hole, and Notched specimens

Specimen	Sample	width (w) [in]	thickness (t) [in]	Modified Width (Circle) (w') [in]	Hole Diameter (d) [in]	Modified Width (Notch) (w') [in]	Notched Thickness (a) [in]	Cross-Sectional Area (in ²)
Control	1	0.453	0.23	--	--	--	--	0.104
	2	0.455	0.231	--	--	--	--	0.105
Circle Hole	1	0.453	0.231	0.213	0.24	--	--	0.0492
	2	0.454	0.23	0.199	0.255	--	--	0.0458
Notched	1	0.453	0.231	--	--	0.237	0.216	0.0499
	2	0.45	0.23	--	--	0.234	0.216	0.0497

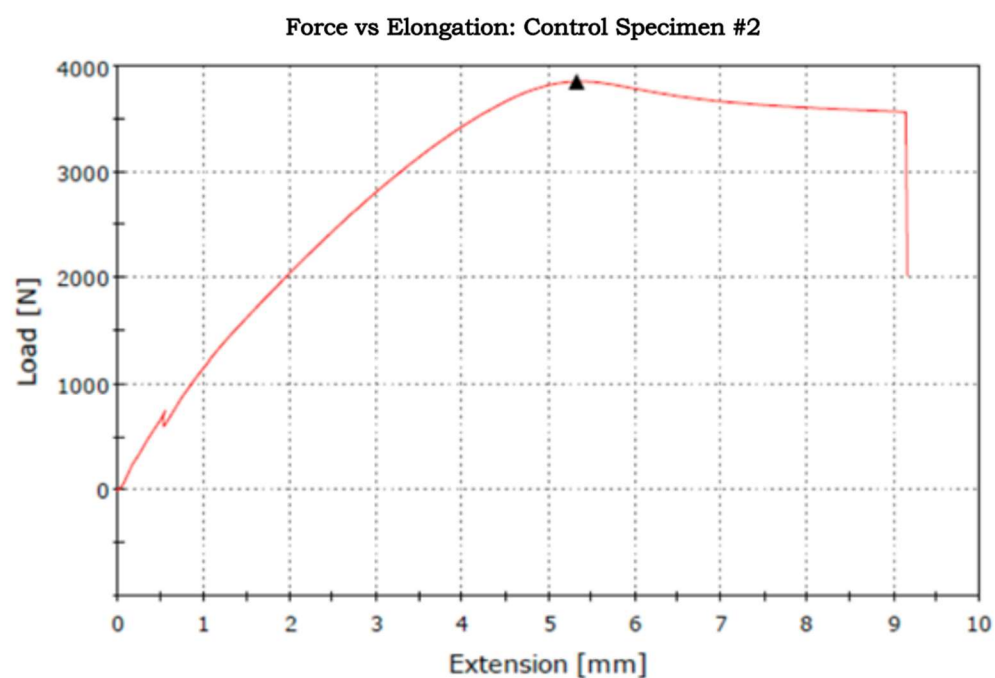
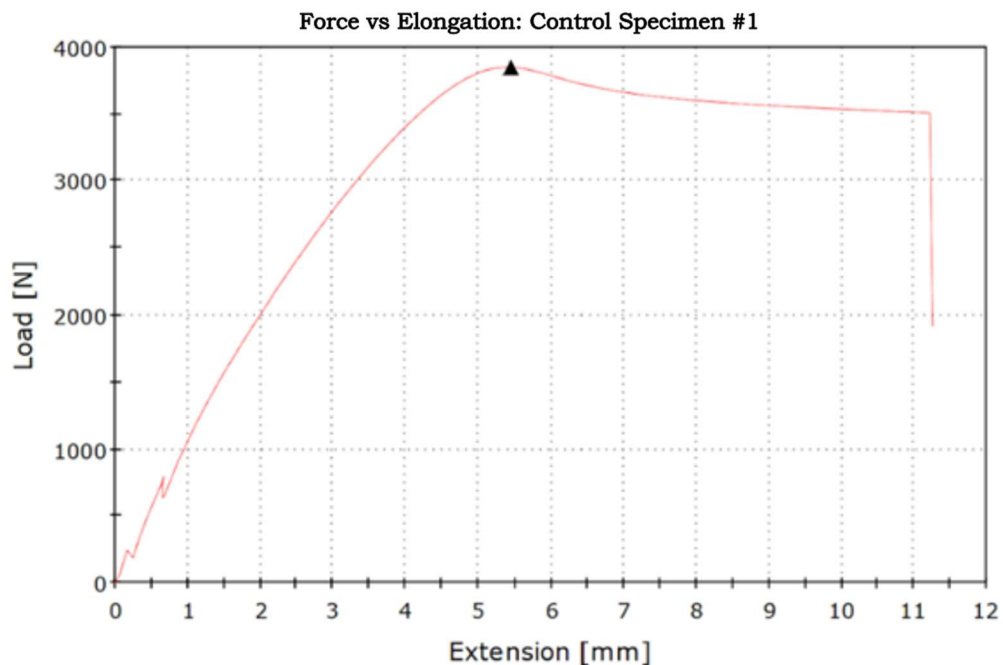
Appendix B

Measured Dimensions and Calculated Cross-Sectional area for Control, Square Hole, and Diamond Hole specimens

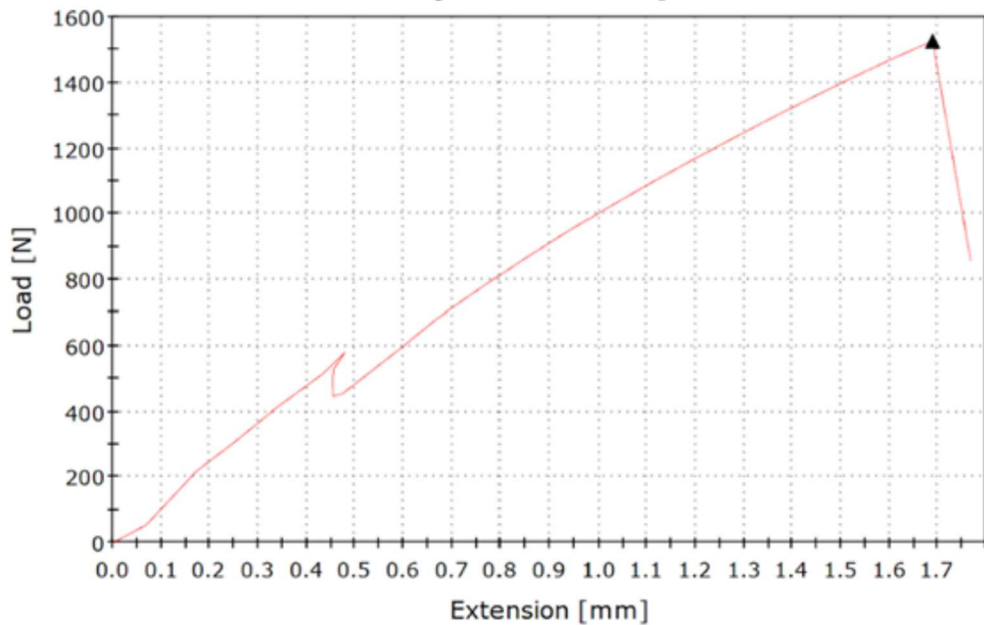
Specimen	Sample	width (w) [in]	thickness (t) [in]	Width (Square Hole) (w') [in]	Modified Width (Square Hole) (w') [in]	Width (Diamond Hole) (w') [in]	Modified Width (Diamond Hole) (w') [in]	Cross-Sectional Area (in ²)
Control	1	0.453	0.23	--	--	--	--	0.104
	2	0.455	0.231	--	--	--	--	0.105
Square Hole	1	0.449	0.23	0.258	0.191	--	--	0.0439
	2	0.453	0.231	0.254	0.199	--	--	0.046
Diamond Hole	1	0.453	0.231	--	--	0.249	0.204	0.0471
	2	0.445	0.23	--	--	0.255	0.19	0.0437

Appendix C

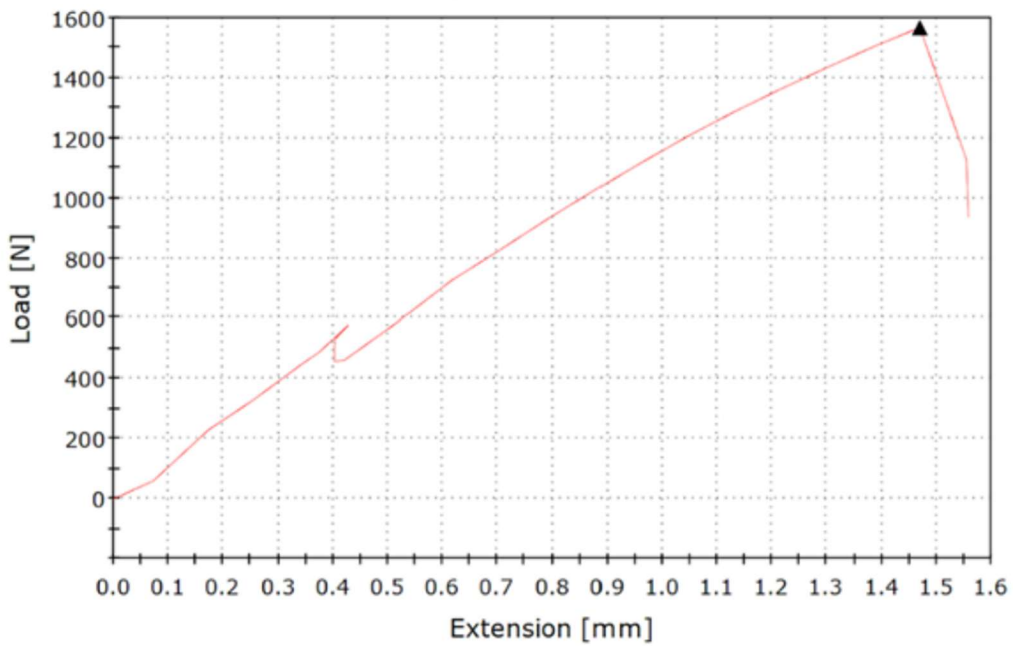
Load vs Elongation Plots for all test specimens



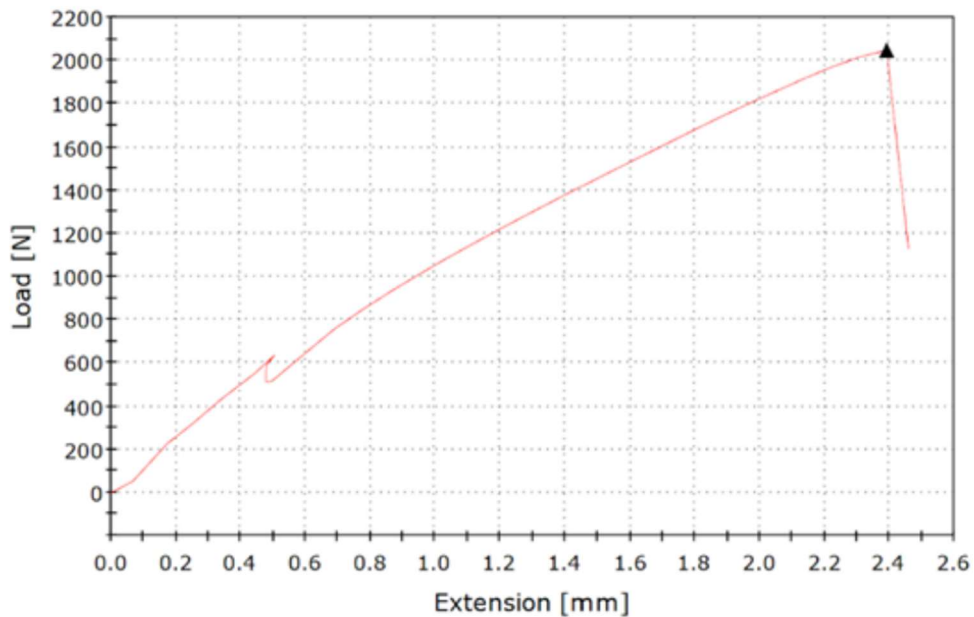
Force vs Elongation: Circle Hole Specimen #1



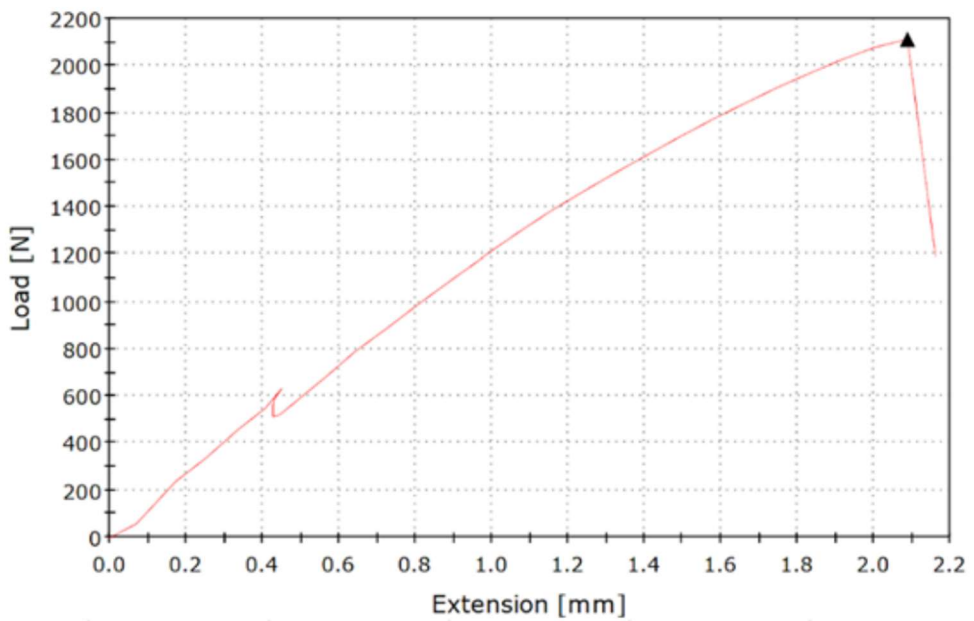
Force vs Elongation: Circle Hole Specimen #2



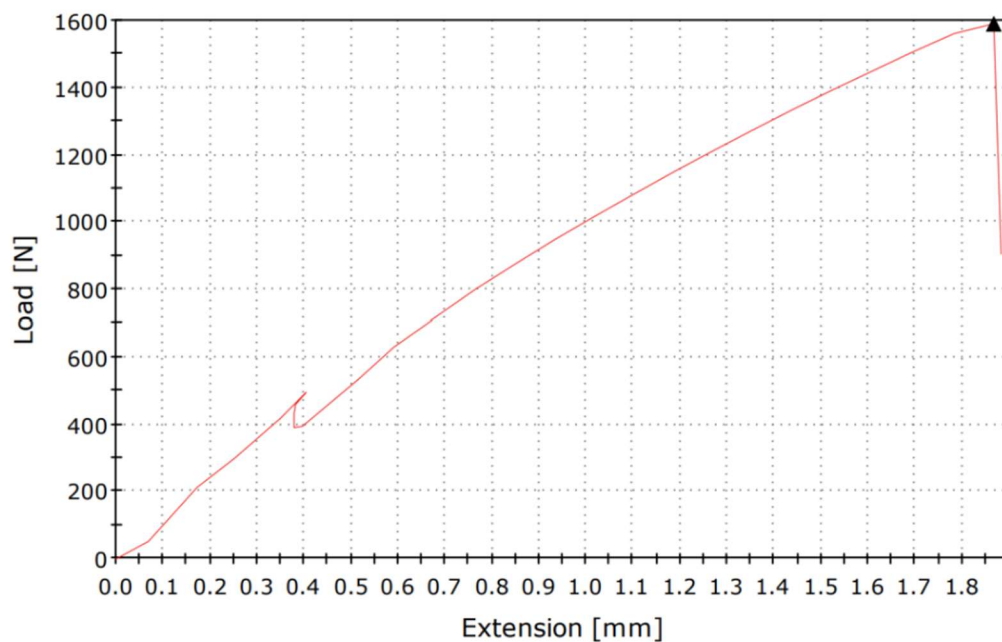
Force vs Elongation: Notched Specimen #1



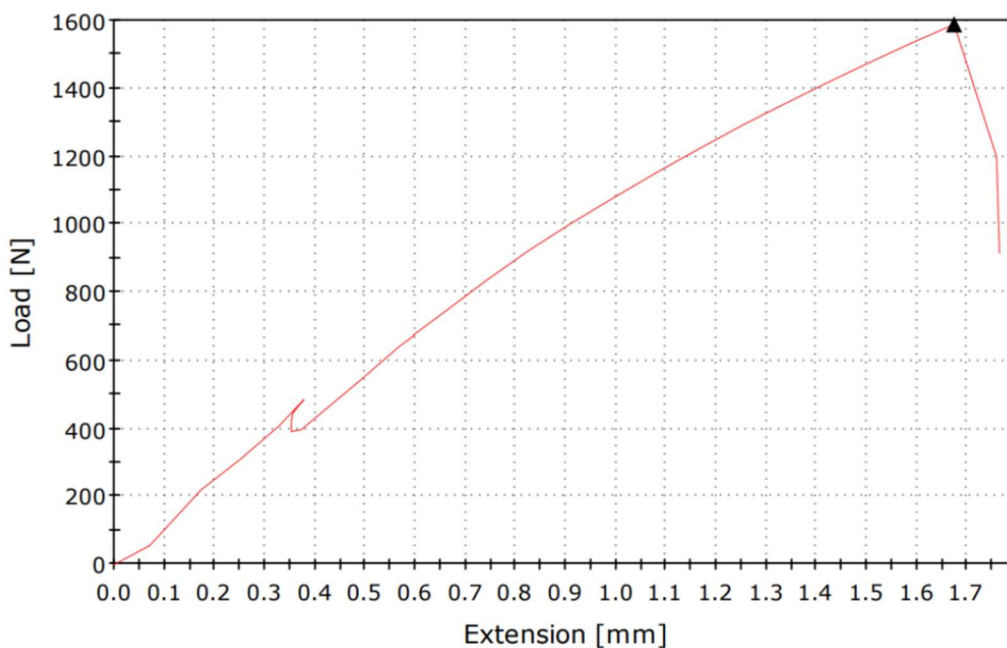
Force vs Elongation: Notched Specimen #2



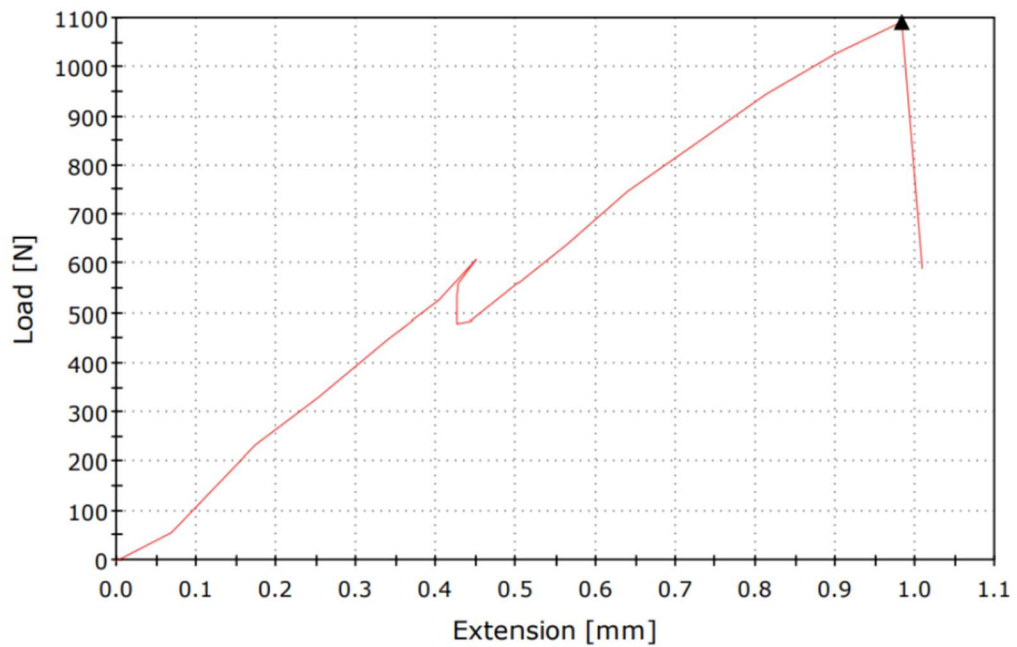
Force vs Elongation: Square Hole Specimen #1



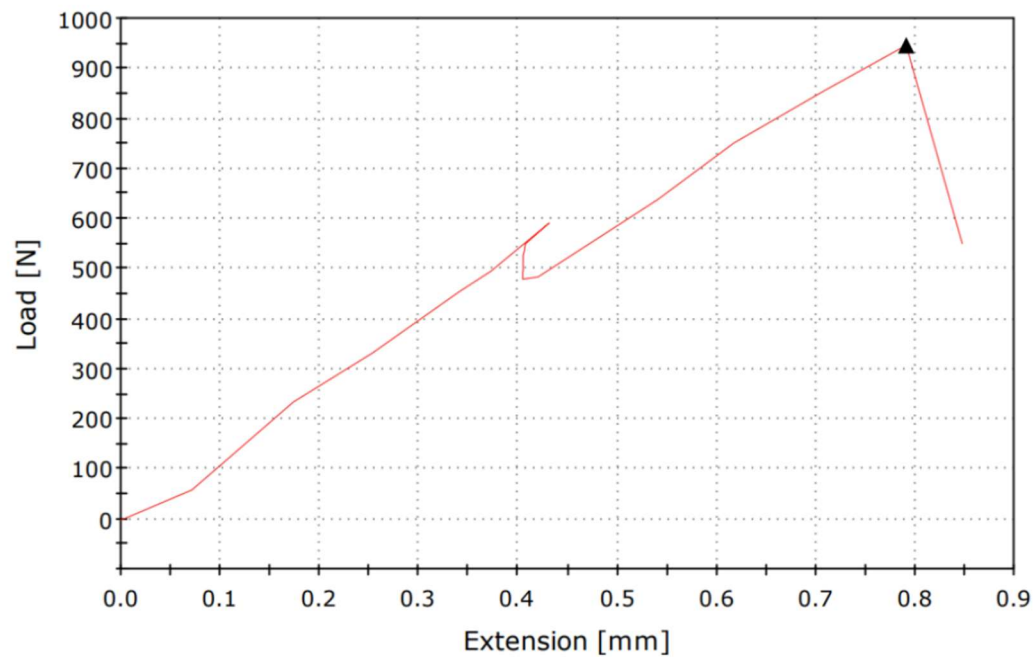
Force vs Elongation: Square Hole Specimen #2



Force vs Elongation: Diamond Hole Specimen #1



Force vs Elongation: Diamond Hole Specimen #2



Appendix D

Hand calculations for various parameters throughout the experiment

Nominal stress (i.e. stress from control)	Theoretical Yield stress for circle Discontinuity
- Sample 1	- Sample 1
$\sigma_{\text{nominal}} = \frac{F}{A} = \frac{750 \text{ N}}{(0.015062 \text{ m} \cdot 0.005842 \text{ m})}$	$K_t = 3 - 3.13 \left(\frac{d}{w} \right) + 3.66 \left(\frac{d}{w} \right)^2 - 1.53 \left(\frac{d}{w} \right)^3$
$\sigma_{\text{nominal}} = 111575.23.03 \text{ Pa}$	$K_t = 3 - 3.13 \left(\frac{6.096}{11.5062} \right) + 3.66 \left(\frac{6.096}{11.5062} \right)^2 - 1.53 \left(\frac{6.096}{11.5062} \right)^3$
$\sigma_{\text{nominal}} = 111575.23.03 \text{ Pa} \cdot \frac{1 \text{ MPa}}{1000000 \text{ Pa}}$	$K_t = 2.14$
$\sigma_{\text{nominal}} = 11.1575 \text{ MPa}$	$\sigma_{\text{max}} = K_t \cdot \sigma_{\text{nominal}}$
- Sample 2	- Sample 2
$\sigma_{\text{nominal}} = \frac{F}{A} = \frac{750 \text{ N}}{(0.015577 \text{ m} \cdot 0.0058674 \text{ m})}$	$\sigma_{\text{max}} = 2.14 \cdot 11.109 \text{ MPa} = 23.79 \text{ MPa}$
$\sigma_{\text{nominal}} = 11060330.32 \text{ Pa}$	-
$\sigma_{\text{nominal}} = 11060330.32 \text{ Pa} \cdot \frac{1 \text{ MPa}}{1000000 \text{ Pa}}$	$K_t = 3 - 3.13 \left(\frac{6.477}{11.5316} \right) + 3.66 \left(\frac{6.477}{11.5316} \right)^2 - 1.53 \left(\frac{6.477}{11.5316} \right)^3$
$\sigma_{\text{nominal}} = 11.06 \text{ MPa}$	$K_t = 2.125$
- Average Nominal stress	$\sigma_{\text{max}} = 2.125 \cdot 11.109 \text{ MPa} = 23.612 \text{ MPa}$
$\sigma_{\text{nominal}} = \frac{(11.1575 \text{ MPa} + 11.06)}{2}$	- Average theoretical Yield stress
$\sigma_{\text{nominal}} = 11.103 \text{ MPa}$	$\sigma_{\text{max}} = \frac{(23.79 \text{ MPa} + 23.612 \text{ MPa})}{2} = 23.701 \text{ MPa}$

Theoretical Yield stress for Notch Discontinuity
- Sample 1
$K_t = C_1 + C_2 \left(\frac{w-d}{w} \right) + C_3 \left(\frac{w-d}{w} \right)^2 + C_4 \left(\frac{w-d}{w} \right)^3$
$C_1 = 0.355 + 2.163 \sqrt{h/r} - 0.081(h/r)$
$= 0.355 + 2.163 \sqrt{\frac{5.4864}{3.2002}} - 0.081 \left(\frac{5.4864}{3.2002} \right)$
$= 3.656$
$C_2 = -1.557 - 4.046 \sqrt{h/r} + 1.032(h/r)$
$= -1.557 - 4.046 \sqrt{\frac{5.4864}{3.2002}} + 1.032 \left(\frac{5.4864}{3.2002} \right)$
$= -5.085$
$C_3 = 4.013 + 0.424 \sqrt{h/r} - 0.748(h/r)$
$= 4.013 + 0.424 \sqrt{\frac{5.4864}{3.2002}} - 0.748 \left(\frac{5.4864}{3.2002} \right)$
$= 3.2858$
$C_4 = -2.461 + 1.538 \sqrt{h/r} - 0.236(h/r)$
$= -2.461 + 1.538 \sqrt{\frac{5.4864}{3.2002}} - 0.236 \left(\frac{5.4864}{3.2002} \right)$
$= -0.8518$
$K_t = 3.656 + 5.085 \left(\frac{11.5062 - 5.4864}{11.5062} \right) + 3.2858 \left(\frac{11.5062 - 5.4864}{11.5062} \right)^2$
$- 0.8518 \left(\frac{11.5062 - 5.4864}{11.5062} \right)^3 = 1.7729$

- Sample 2

$$K_t = C_1 + C_2 \left(\frac{w-d}{w} \right) + C_3 \left(\frac{w-d}{w} \right)^2 + C_4 \left(\frac{w-d}{w} \right)^3$$

$$\begin{aligned} C_1 &= 0.955 + 2.169 \sqrt{\frac{h/r}{3.2002}} - 0.081 \left(\frac{h/r}{3.2002} \right) \\ &= 0.955 + 2.169 \sqrt{\frac{5.4864}{3.2002}} - 0.081 \left(\frac{5.4864}{3.2002} \right) \\ &= 3.656 \end{aligned}$$

$$\begin{aligned} C_2 &= -1.557 - 4.046 \sqrt{\frac{h/r}{3.2002}} + 1.032 \left(\frac{h/r}{3.2002} \right) \\ &= -1.557 - 4.046 \sqrt{\frac{5.4864}{3.2002}} + 1.032 \left(\frac{5.4864}{3.2002} \right) \\ &= -5.085 \end{aligned}$$

$$\begin{aligned} C_3 &= 4.053 + 0.424 \sqrt{\frac{h/r}{3.2002}} - 0.748 \left(\frac{h/r}{3.2002} \right) \\ &= 4.053 + 0.424 \sqrt{\frac{5.4864}{3.2002}} - 0.748 \left(\frac{5.4864}{3.2002} \right) \\ &= 3.2858 \end{aligned}$$

$$\begin{aligned} C_4 &= -2.461 + 1.638 \sqrt{\frac{h/r}{3.2002}} - 0.236 \left(\frac{h/r}{3.2002} \right) \\ &= -2.461 + 1.638 \sqrt{\frac{5.4864}{3.2002}} - 0.236 \left(\frac{5.4864}{3.2002} \right) \\ &= -0.8518 \end{aligned}$$

$$\begin{aligned} K_t &= 3.656 - 5.085 \left(\frac{11.43 - 5.4864}{11.43} \right) + 3.2858 \left(\frac{11.43 - 5.4864}{11.43} \right)^2 \\ &\quad - 0.8518 \left(\frac{11.43 - 5.4864}{11.43} \right)^3 \\ &= 1.7804 \end{aligned}$$

$$T_{max} = K_t \cdot T_{nominal}$$

$$= 1.7804 \cdot 11.109 \text{ MPa}$$

$$= 19.778 \text{ MPa}$$